

# Breach in the Shield: Unveiling the Vulnerabilities of Large Language Models

Runpeng Dai\*

Department of Biostatistics  
University of North Carolina at Chapel Hill  
Chapel Hill, NC, USA  
runpeng@unc.edu

Fan Zhou<sup>†</sup>

Department of Statistics and Management  
Shanghai University of Finance and Economics  
Shanghai, China  
zhoufan@mail.shufe.edu.cn

Run Yang\*

Department of Statistics and Management  
Shanghai University of Finance and Economics  
Shanghai, China  
runyang@mail.shufe.edu.cn

Hongtu Zhu<sup>†</sup>

Department of Biostatistics  
University of North Carolina at Chapel Hill  
Chapel Hill, NC, USA  
htzhu@email.unc.edu

## Abstract

Large Language Models (LLMs) and Vision-Language Models (VLMs) have become essential to general artificial intelligence, exhibiting remarkable capabilities in task understanding and problem-solving. However, the real-world reliability of these models critically depends on their stability, which remains an underexplored area. Despite their widespread use, rigorous studies examining the stability of LLMs under various perturbations are still lacking. In this paper, we address this gap by proposing a novel stability measure for LLMs, inspired by statistical methods rooted in information geometry. Our measure possesses desirable invariance properties, making it well-suited for analyzing model sensitivity to both parameter and input perturbations. To assess the effectiveness of our approach, we conduct extensive experiments on models ranging in size from 1.5B to 13B parameters. Our results demonstrate the utility of our measure in identifying salient parameters and detecting vulnerable regions in input images or critical dimensions in token embeddings. Furthermore, leveraging our stability framework, we enhance model robustness during model merging, leading to improved performance.

## Keywords

Large Language Models, Stability Measure

### ACM Reference Format:

Runpeng Dai, Run Yang, Fan Zhou, and Hongtu Zhu. 2025. Breach in the Shield: Unveiling the Vulnerabilities of Large Language Models. In . ACM, New York, NY, USA, 10 pages. <https://doi.org/10.1145/nnnnnnn.nnnnnnn>

\*Both authors contributed equally to this research.

<sup>†</sup>Corresponding author.

Permission to make digital or hard copies of all or part of this work for personal or classroom use is granted without fee provided that copies are not made or distributed for profit or commercial advantage and that copies bear this notice and the full citation on the first page. Copyrights for components of this work owned by others than the author(s) must be honored. Abstracting with credit is permitted. To copy otherwise, or republish, to post on servers or to redistribute to lists, requires prior specific permission and/or a fee. Request permissions from [permissions@acm.org](mailto:permissions@acm.org).  
*Conference'17, Washington, DC, USA*

© 2025 Copyright held by the owner/author(s). Publication rights licensed to ACM.  
ACM ISBN 978-x-xxxx-xxxx-x/YYYY/MM  
<https://doi.org/10.1145/nnnnnnn.nnnnnnn>

## 1 Introduction

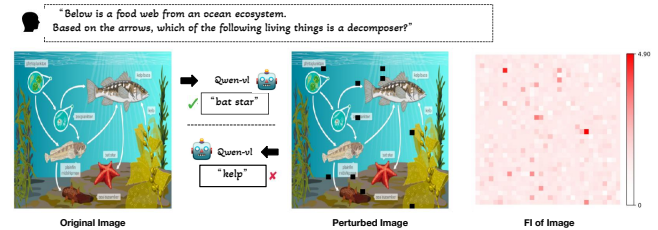


Figure 1: A case study of the Qwen-VL model on the SCI-QA. The image on the far right shows the per-pixel FI values calculated for this case, while the middle image illustrates how perturbing the top 10 positions with the highest FI values induces hallucination

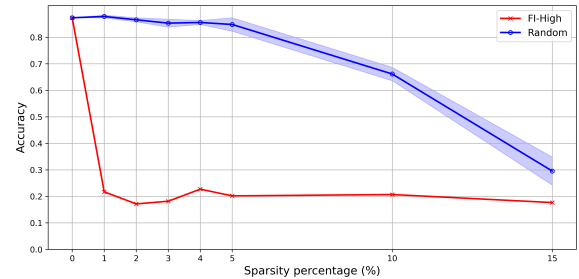


Figure 2: A case study of the Qwen2 on the MMLU-geography. The figure illustrates the accuracy of responses to multiple-choice problems as an increasing percentage of parameters are zeroed out. “FI-High” denotes zeroing out parameters with high FI values, while “Random” represents randomly zeroing out parameters.

Large Language Models (LLMs) and Vision Language Models (VLMs) such as GPT [6] and Llama [43], have revolutionized the field of Natural Language Processing (NLP), exhibiting remarkable proficiency across a variety of tasks [1, 21] and modalities [3, 28].

These modern LLMs are massive in size, trained on vast amounts of data, and meticulously aligned to prevent from generating harmful content [36], leaking private information [53], or exhibiting sexual or religious bias [46].

Despite the enthusiasm for these integrative approaches, a critical issue remains: LLMs remain susceptible to both external and internal perturbations, affecting their reliability and performance.

**Externally**, LLMs are vulnerable to input perturbations, such as Embedding-Corrupted Prompts [14, 27]. This susceptibility extends to visual inputs in VLMs, where adversarially optimized images can drastically alter model behavior [37]. Beyond adversarial attacks, VLMs exhibit high sensitivity to perturbations in specific local regions of an image—a common issue, as user-uploaded images often suffer from blurring, masking, or low resolution.

Our case study on the Qwen-VL model [3] highlights this vulnerability. We applied our proposed stability measure to each pixel in the input image, as shown in the right columns of Figure 1. Based on these calculations, we masked the top 10 most sensitive patches irrelevant to the prompt question, which effectively misled the model into generating incorrect responses.

**Internally**, LLM stability is further challenged by parameter perturbations, often introduced through quantization and model merging. While these techniques improve deployment efficiency by reducing inference costs [2, 15], they can also induce hallucinations and degrade performance [25, 34, 51].

Not all parameters are equally susceptible. As shown in Figure 2, the model retains similar performance even when 5% of randomly selected parameters are dropped. However, zeroing out just 1% of the parameters with the highest Fisher Information (FI) can reduce accuracy below random guessing (0.25), highlighting the critical role of identifying these vulnerable locations.

To address these challenges, we propose a novel stability measure called **FI**, First order local Influence, to quantitatively assess the stability of LLMs against local perturbations. Specifically, we construct a perturbation manifold that encompasses all perturbed models, along with its associated geometric properties. Our stability measure quantifies the degree of local influence of the perturbation to a given objective function within this manifold and thus reflects the stability of each component of LLMs.

This measure is highly versatile, effectively assessing model stability under both external and internal perturbations across various levels of granularity—from individual parameters to input features such as pixels and patches.

Existing approaches, such as the Jacobian norm [35] and Saliency Map [41], can also serve as stability measures for large language models. We set these methods as competing baselines and conduct various numerical analyses to demonstrate the advantages of our approach. Moreover, among all these methods, ours is the only one that remains invariant to parameter reparameterization, a crucial property for interpretability, as discussed in Section 3.

We conduct extensive studies to validate our method in identifying fragile pixels in vision inputs of VLMs (Subsections 4.1 and 4.2), vulnerable embedding dimensions of tokens in LLMs (Subsection 4.3), and salient parameters across models of varying sizes (Subsection 5.1).

Furthermore, we integrate our measure into various model merging methods (Subsection 5.2), demonstrating that protecting salient

parameters with high FI values can significantly mitigate degradation caused by model merging, underscoring the critical role of FI in optimizing model performance.

Our main contributions are summarized as follows:

- (i) We propose a novel framework that assesses the stability of individual components within LLMs, quantifying the impact of small perturbations on the overall system.
- (ii) We conduct experiments on multiple datasets spanning vision-language models and large language models. The results consistently demonstrate the effectiveness of our approach in identifying both external and internal vulnerabilities.
- (iii) We leverage stability measure to design a parameter protection mechanism that improves the performance of various model merging techniques, demonstrating the practical value of our stability measure. algorithms.

## 2 Related Work

**LLM Jailbreak.** Prior work on LLM jailbreaking has mainly focus on the power of adversarially optimizing toward a prompt that elicits a desired LLM response [14, 17, 26, 57]. Previous studies [19, 52] have highlighted that specific prompts, suffixes, and even so-called "magic code" [30] can induce inappropriate or harmful behaviors in language models. Recently [14] have found that the attack can be simplified to learning perturbation vectors added to the token embeddings, which eliminates the need to optimize over discrete tokens. [17, 27] show similar results that manipulates embeddings could elicit refusal behavior or incorrect answers from an instruction-tuned LLM. However, the aforementioned approaches mainly focus on jailbreaking methodologies and rely on empirically specifying the target dimensions for perturbation.

**VLMs Jailbreak.** Despite achieving impressive performance, VLMs still face issues of adversarial robustness [42]. Multiple attempts have been conducted to study the robustness of VLMs from different aspects. [54] evaluates the adversarial robustness of MLLMs on image captioning under white-box settings, while [39] conducts both transfer-based and query-based attacks on MLLMs assuming black-box access. [7, 38] trigger VLMs to generate toxic content by imposing adversarial perturbations to the input images. [4] studies image hijacks to achieve specific string, leak context, and jailbreak attacks. These exploratory works demonstrate that MLLMs still face stability and security issues under adversarial perturbations.

## 3 Local Stability Measure of Large language models

In this section, we propose a new metric called FI to quantify the stability of large language models against local perturbations. Specifically, we focus on auto-regressive language models, which generate one token at a time based on both the initial input and previously generated tokens. Considering this sequential generation nature, we first develop FI for single-step token generation tasks and discuss its theoretical and computational properties in great detail. Following this, we demonstrate how the proposed stability measure can be naturally extended to address sequence generation tasks.

**Problem formulation.** Consider an LLM parameterized by  $\theta$ , with input data  $x$ , which may consist of text or, for visual language models, a combination of text and images. Given  $x$ , the model generates a probability distribution over its vocabulary to predict the next token, which can be framed as a classification problem with  $K$  classes, where  $K$  represents the vocabulary size.

However, vocabulary sizes are typically large [3, 11], and predictions are often concentrated on a small subset of tokens. Instead of using the entire vocabulary, it is more efficient to focus on a relevant subset based on the task. For example, in multiple-choice questions, probabilities are restricted to the choices "A", "B", "C", or "D". Classes can also be defined semantically, such as categorizing tokens as "neutral" or "notorious" in toxicity detection [16].

With appropriately defined classes, the predicted probability for class  $y \in \{1, \dots, K\}$  is denoted as  $P(y|x, \theta)$ , satisfying  $\sum_{y=1}^K P(y|x, \theta) = 1$ . Let  $\omega \in \mathbb{R}^d$  be a perturbation vector varies in an open subset  $\Omega$ .  $\omega$  can be applied to a subset of the model parameters  $\theta$  and locations within the input data  $x$ . We denote the output of the perturbed model under this perturbation as  $P(y|x, \theta, \omega)$ .

**FI metric.** Since our primary interest lies in examining the behavior of  $P(y|x, \omega, \theta)$  as a function of  $\omega$  near  $\omega_0 = 0$ , we shift focus from  $\theta$  to  $\omega$ . We introduce the perturbation manifold as defined in [55] and [56].

**DEFINITION 3.1.** Define the  $d$ -dimensional perturbation manifold  $\mathcal{M} = \{P(y|x, \theta, \omega) : \omega \in \Omega\}$ , which encompasses all perturbed models. Assume that for all  $\omega \in \Omega$ , the perturbed models  $\{P(y = i|x, \theta, \omega)\}_{i=1}^K$  are positive and sufficiently smooth. The tangent space  $T_\omega$  of  $\mathcal{M}$  at  $\omega$  is spanned by the partial derivatives of the log-likelihood function  $\ell(\omega|y, x, \theta) = \log P(y|x, \theta, \omega)$  with respect to  $\omega$ , specifically  $T_\omega = \text{span}\{\frac{\partial}{\partial \omega_i} \ell(\omega|y, x, \theta)\}_{i=1}^d$ .

The metric  $g_\omega$  on  $\mathcal{M}$  can be defined with the metric tensor  $G_\omega$ . Consider two tangent vectors at  $\omega$  given by

$$v_j(\omega) = h_j^\top \partial_\omega \ell(\omega|y, x, \theta) \in T_\omega, \quad j = 1, 2$$

where  $h_1, h_2$  are the weights on the basis. Their inner product is defined as:

$$\langle v_1(\omega), v_2(\omega) \rangle_{g_\omega} = \sum_{y=1}^K v_1(\omega) v_2(\omega) P(y|x, \theta) = h_1^\top G_\omega h_2.$$

The metric tensor  $G_\omega$  is given by:

$$G_\omega = \sum_{y=1}^K \partial_\omega \ell(\omega|y, x, \theta) \partial_\omega^\top \ell(\omega|y, x, \theta) P(y|x, \theta, \omega).$$

Subsequently, the norm of  $v_j(\omega)$  under metric  $g_\omega$  is:

$$\|v_j\|_{g_\omega} = \sqrt{h_j^\top G_\omega h_j}.$$

Let  $C(t) = P(y|x, \theta, \omega(t))$  be a smooth curve on the manifold  $\mathcal{M}$  connecting two points  $\omega_1 = \omega(t_1)$  and  $\omega_2 = \omega(t_2)$ . Then, the distance between  $\omega_1$  and  $\omega_2$  along the curve  $C(t)$  is given by:

$$\begin{aligned} S_C(\omega_1, \omega_2) &= \int_{t_1}^{t_2} \sqrt{\|\partial_t \log P(y|x, \theta, \omega(t))\|_{g_\omega}} dt \\ &= \int_{t_1}^{t_2} \sqrt{\frac{d\omega(t)^\top}{dt} G_{\omega(t)} \frac{d\omega(t)}{dt}} dt. \end{aligned} \quad (1)$$

With the Perturbation manifold  $\mathcal{M}$  and respective metric  $g_\omega$  defined, we are ready to propose the metric that quantifies the stability of large language models (LLMs) against various types of local perturbations. Let  $f(\omega)$  be the objective function of interest for sensitivity analysis, in our case being  $-\log P(y_{pred}|x, \theta, \omega)$ , we can define the following (first-order) local influence metric FI:

**DEFINITION 3.2.** Given the perturbation manifold  $\mathcal{M}$  and its metric, the first-order local stability measure of  $f(\omega)$  at  $\omega(0) = \omega_0$  is defined as

$$FI_\omega(\omega_0) = \max_C \lim_{t \rightarrow 0} \frac{[f(\omega(t)) - f(\omega(0))]^2}{S_C^2(\omega(t), \omega(0))}. \quad (2)$$

The ratio in Equation 2 measures the amount of change introduced to the objective function relative to the distance of the perturbation on the perturbation manifold. Thus, Equation 2 can be naturally interpreted as the maximum local ratio of change among all possible perturbation curves  $C(t)$ . The proposed FI measure has the property of transformation invariance.

**THEOREM 3.3 (REPARAMETRIZATION INVARIANCE).** Suppose that  $\phi$  is a diffeomorphism of  $\omega$ . Then,  $FI_\omega(\omega_0)$  is invariant with respect to any reparameterization corresponding to  $\phi$ . Specifically, let

$$\tilde{\omega}(t) = \phi \circ \omega(t), \quad \tilde{\omega}_0 = \phi(\omega_0),$$

we have

$$FI_{\tilde{\omega}}(\tilde{\omega}_0) = FI_\omega(\omega_0).$$

The detailed proof can be found in [40].

Theorem 3.3 establishes that  $FI_\omega(\omega_0)$  is invariant under any diffeomorphic (e.g., scaling and spinning) reparameterization of the original perturbation. This invariance property is not shared by other measures, such as Jacobian norm [35], Cook's local influence measure [9], and Sharpness [35].

For instance, consider a perturbation of the form  $\alpha + \Delta\alpha$ , where  $\alpha$  is a subvector of  $(x^\top, \theta^\top)^\top$ . If we apply a scaling reparameterization  $\alpha' = K \odot \alpha$ , where  $K$  is a scaling vector and  $\odot$  denotes element-wise multiplication, then the Jacobian norms change:

$$\|J(\alpha)\|_F = \left[ \sum_i \left( \frac{\partial f}{\partial \alpha_i} \right)^2 \right]^{1/2} \neq \|J(\alpha')\|_F.$$

In contrast, the FI measure remains unchanged. Such a reparameterization does not alter the function itself but may affect the measure values, potentially weakening the correlation between perturbation and performance degradation. A similar discussion can be found in [10].

**Computation of FI.** As we will show, Theorem 3.3 on diffeomorphic reparameterization invariance enables us to derive an easy-to-compute solution for Equation 2, while addressing the low-dimensionality problem inherent in LLMs.

**THEOREM 3.4.** If  $G_\omega$  is positive definite, the FI measure has the following closed-form:

$$FI_\omega(\omega_0) = \nabla_{f(\omega_0)}^\top G_{\omega_0}^{-1} \nabla_{f(\omega_0)}, \quad (3)$$

where

$$\nabla_{f(\omega_0)} = \left. \frac{\partial f(\omega)}{\partial \omega} \right|_{\omega=\omega_0}.$$

The detailed proof of Theorem 3.4 can be found in Appendix A.3. It is important to note that the closed form of FI in Theorem 3.4 depends on the positive definiteness of  $G_\omega$ , which is not always guaranteed. This is due to the fact that the parameters in LLMs are often high-dimensional tensors with low-rank structures [22].

Motivated by [40], we apply the invariant Theorem 3.3 by transforming  $\omega$  to a vector  $v$  such that  $G_v = \mathbf{I}_K$ , where  $K$  is an integer. Specifically, we notice that

$$G_{\omega_0} = B_0^T B_0,$$

where

$$B_0 = \left[ P(y = i|x, \theta, \omega)^{1/2} \partial_\omega \ell(\omega|y = i, x, \theta) \right]_{1 \leq i \leq K}.$$

Let  $r_0 = \text{rank}(G_{\omega_0})$ , we apply the compact SVD to  $B_0 \in \mathbb{R}^{p \times K}$ , which yields:

$$B_0 = V_0 \Lambda_0 U_0,$$

where  $V_0 \in \mathbb{R}^{p \times r_0}$  and  $U_0 \in \mathbb{R}^{r_0 \times K}$  are semi-orthogonal matrices and  $\Lambda_0 \in \mathbb{R}^{r_0 \times r_0}$  is a diagonal matrix. Under the transformation  $v = \Lambda_0 V_0^T \omega$ , we have

$$\begin{aligned} \mathbf{FI}_\omega(\omega_0) &= \mathbf{FI}_v(v_0) \\ &= \nabla_{f(v_0)}^\top \nabla_{f(v_0)} \\ &= \nabla_{f(\omega_0)}^\top (V_0 R_0)^\top \Lambda_0^{-2} (V_0 R_0) \nabla_{f(\omega_0)}. \end{aligned} \quad (4)$$

where the second equality holds by applying the chain rule to  $G_v$ .

**Average FI.** Since the perturbation manifold  $\mathcal{M}$  depends on the input data  $x$ , FI is inherently a data-dependent measure. To make this dependence explicit, we denote  $\mathbf{FI}_\omega(\omega_0)$  as  $\mathbf{FI}(x, \theta, \omega)$ . In analyses focusing on individual cases, such as pixel vulnerability analysis, where  $\omega$  represents a subset of the input data  $x$ , a data-dependent stability measure suffices. However, when the focus shifts to assessing the stability of the model parameters alone, a data-independent measure is required.

To address this, we follow the approach of other stability metrics like the Jacobian norm [35] and define the average FI as  $\mathbb{E}_{P_x} [\mathbf{FI}(x, \theta, \omega)]$ , where  $P_x$  represents the distribution of the input data  $x$ . Given a pre-collected dataset  $\mathcal{D} = \{x_1, \dots, x_n\}$  with  $x_i \sim P_x$ , the average FI can be approximated by the empirical FI:  $\mathbb{E}_{\hat{P}_x} [\mathbf{FI}(x, \theta, \omega)] = n^{-1} \sum_{i=1}^n \mathbf{FI}(x_i, \theta, \omega)$ , where  $\hat{P}_x$  denotes the empirical distribution of  $x$  based on the dataset  $\mathcal{D}$ .

**FI for sequence generation.** Sequence generation is essentially multiple rounds of next-token generation, where the  $l$ -th token  $y^{(l)}$  is generated given the initial input  $z$  and previously generated tokens  $\{y^{(1)}, \dots, y^{(l-1)}\}$ . We define the FI measure for generating the  $l$ -th token  $y^{(l)}$  given the initial input  $z$  by averaging out the randomness from the preceding steps

$$\mathbf{FI}_l(z) = \mathbb{E}_{y^{(1)}, \dots, y^{(l-1)}} \left[ \mathbf{FI}(\{z, y^{(1)}, \dots, y^{(l-1)}\}, \theta, \omega) \right]. \quad (5)$$

To formulate an overall measure for sequence generation, we aggregate these per-token FI measures. Since sequences generated by LLMs can vary in length, we propose two methods to handle

this heterogeneity. The first approach sets a fixed horizon  $L$  and computes the mean FI over these rounds

$$\mathbf{FI}_{\text{seq}}^L(z) = \frac{1}{L} \sum_{l=1}^L \mathbf{FI}_l(z). \quad (6)$$

Alternatively, inspired by the concept of average discounted rewards in reinforcement learning [29], we consider sequences of potentially infinite length and propose a discounted FI measure with discount factor  $\gamma$

$$\mathbf{FI}_{\text{seq}}^{\infty, \gamma}(z) = (1 - \gamma) \sum_{l=0}^{\infty} \gamma^l \cdot \mathbf{FI}_l(z).$$

By taking the expectation over the distribution of  $z$ , we obtain the average FI for sequence generation in both cases  $\mathbb{E}_{P_z} [\mathbf{FI}_{\text{seq}}^L(z)]$  and  $\mathbb{E}_{P_z} [\mathbf{FI}_{\text{seq}}^{\infty, \gamma}(z)]$ , respectively.

## 4 External perturbations analysis

In this section, we begin with a case study to demonstrate how FI can be used to identify fragile pixels in VLMs. We then compare FI with other stability measures in designing adversarial attacks on both vision and language inputs of LLMs/VLMs. Finally, we present experiments highlighting the potential applications of FI in cross-modal analysis.

### 4.1 Detection of fragile pixels

Let  $X$  be an image input to a VLM with RGB channels. Given the input  $X$  the VLM outputs the prediction probability for each of the choice  $y \in \{1, \dots, 4\}$  denoted by  $P(y|x, \theta)$  and pick  $y_{\text{pred}} = \arg \max_y P(y|x, \theta)$  as its answer.

Let  $\omega_i \in \mathbb{R}^3$  denote the perturbation vector to the  $i$ -th pixel, we focus the influence of that perturbation to the entropy of the prediction, defined as  $f(x) = -\log P(y_{\text{pred}}|x, \theta)$ .

Specifically, the experiment is conducted using a multiple-choice problem sampled from the ScienceQA dataset [32] with the Qwen-VL model. In Figure 1, we calculated the FI values for each pixel using Equation 4. The FI intensity of each pixel is displayed in the image on the far right. Notably, some pixels exhibit significantly higher FI values compared to others.

As shown in the right columns of Figure 1, the overall distribution of FI values across the pixels is non-uniform. The FI values in the background regions are relatively low, ranging between 0 and 1, while the FI values around relevant objects, such as the kelp and starfish, are comparatively higher, with certain regions reaching up to 4.9. However, not all areas covering these relevant objects are equally vulnerable. This phenomenon suggests that the model exhibits heightened sensitivity to perturbations in specific patches, rather than uniformly across the entire object.

To further investigate, we perturb the image by masking the top-10 FI value patches, as shown in the middle column of Figure 1. This perturbation does not cause the model to lose the essential information regarding the food chain relationships necessary to answer the question, but it still induces hallucinations. The model shifts from confidently providing the correct answer—bat star ( $p = 0.72$ ) and kelp ( $p = 0.28$ )—to a less confident and incorrect response—bat

star ( $p = 0.43$ ) and kelp ( $p = 0.57$ ). This empirical finding demonstrates the usefulness of FI in detecting vulnerable inputs for VLMs, suggesting that more robust training methods can be developed by focusing on these sensitive regions.

## 4.2 VLMs Sensitivity Analysis benchmark

To demonstrate the effectiveness of our method, we compare it against state-of-the-art approaches, including Jacobian-Norm [35] and Saliency-Map [44]. Specifically, we conduct the attack process on the MMBench dataset [31], a comprehensive benchmark designed to evaluate various multi-modal capabilities of VLMs. For a fair comparison, we identify the top 10 patches using these methods and assess the model’s performance after masking out the corresponding pixels. The experiments were conducted on the Qwen-vl model.

From Table 2, we observe that, in most cases, masking out pixels identified by the FI measure leads to the most significant performance degradation, clearly demonstrating the superiority of FI over baseline methods. Notably, even in question categories where the model initially performs well, the FI method more precisely identifies unstable positions, effectively disrupting the model’s performance. This suggests that possessing more accurate knowledge does not necessarily ensure stability.

**Table 1: Comparison of accuracy in the MMLU dataset after perturbing the same number of dimensions in the embedding space identified using different methods. The worse the performance, the more it proves that the sensitive dimension has been correctly identified.**

Model	Method	Business	Geography	Culture	Law
Pythia-70M	Saliency-Map	<b>0.002</b>	0.08	<b>0.055</b>	0.13
	Jacobian-Norm	0.113	0.1	0.15	0.13
	FI (ours)	0.110	<b>0.03</b>	0.155	<b>0.11</b>
Pythia-160M	Saliency-Map	0.225	0.24	0.2	0.18
	Jacobian-Norm	0.146	0.24	0.21	0.18
	FI (ours)	<b>0.15</b>	<b>0.22</b>	<b>0.195</b>	<b>0.163</b>
Pythia-410M	Saliency-Map	0.284	0.236	0.26	0.278
	Jacobian-Norm	0.279	0.231	0.22	0.265
	FI (ours)	<b>0.273</b>	<b>0.22</b>	<b>0.21</b>	<b>0.26</b>
Pythia-1B	Saliency-Map	0.278	0.272	0.21	0.243
	Jacobian-Norm	0.273	0.264	0.201	0.241
	FI (ours)	<b>0.270</b>	<b>0.261</b>	<b>0.195</b>	<b>0.236</b>

## 4.3 LLMs Sensitivity Analysis benchmark

In this section, we conduct adversarial attack experiments on pure-text LLMs to verify the effectiveness of our approach in identifying vulnerable embedding dimensions. Specifically, we follow the token embedding attack methods proposed in [27] and [14].

More concretely, for the first token of each prompt, we compute sensitivity using Jacobian-Norm, Saliency Map, and FI, respectively. Then, we adopt the gradient-based attack strategy from [14], i.e., obtaining the attack vector by minimizing  $-\log P(y_{\text{pred}}|x, \theta)$ . The attack is applied along the most sensitive dimensions identified by each method. Specifically, we perturb only the top 0.1% most

sensitive dimensions within the token embedding space. This ensures that the attack remains targeted while effectively revealing instability in different model architectures.

The experiments were conducted on the Pythia [5] models of different sizes. The results, as shown in Table 1, demonstrate the effectiveness of the FI method in identifying and attacking the most sensitive dimensions. The results indicate that FI consistently outperforms both Jacobian-Norm and Gradient-based methods in detecting instability, particularly in smaller models like Pythia-70M and Pythia-160M. Furthermore, unlike the Saliency-Map, which exhibits instability (e.g., an extremely low sensitivity score in Pythia-70M’s Business domain), FI provides more reliable and consistent results across all model scales. These findings suggest that FI offers a more precise and scalable approach for sensitivity analysis, effectively capturing vulnerabilities while maintaining attack efficiency.

**Table 2: Comparison of accuracy in the MMBench dataset after masking the same number of patches in images identified using different methods. The worse the performance, the more it proves that the sensitive patches have been correctly identified.**

Methods	Action Recognition	Attribute Comparison	Attribute Recognition	Celebrity Recognition	Function Reasoning
FI (Ours)	<b>0.32</b>	0.46	<b>0.40</b>	<b>0.67</b>	<b>0.41</b>
Jacobian-Norm	0.66	<b>0.43</b>	0.58	0.90	0.60
Saliency-Map	0.78	0.55	0.52	0.87	0.63
Baseline	0.81	0.56	0.54	0.88	0.68

## 4.4 Cross-Modal Analysis

To gain deeper insight into how prompt engineering affects model stability, we conducted experiments to explore the impact of different prompt engineering strategies.

We defined two distinct types of prompt settings:

- The "aggressive" prompt, such as *"Please consider every detail in the image,"* aims to enhance the model’s focus on finer details.
- The "safe" prompt, such as *"Please focus on the entities and relationships in the image, rather than the noise or potential masks,"* reduces the model’s attention to irrelevant noise.

We computed the Feature Importance (FI) value for each pixel and visualized how these values are distributed under different prompt settings. As illustrated in the left column of Figure 3, the FI values clearly reflect the prompt instructions. The "aggressive" prompt shifts the FI distribution to higher values, with a noticeable increase in both the mean and maximum FI values, indicating that the model becomes more sensitive to pixel-level perturbations across the image. Conversely, the "safe" prompt significantly shifts the FI distribution toward lower values, indicating reduced sensitivity and enhanced stability against perturbations in less relevant areas.

However, neither prompt fully guarantees model stability. As depicted in the right column of Figure 3, overlaying the FI values obtained under the "safe" prompt onto the image reveals that while the model adheres to the prompt by reducing its sensitivity to the background, it remains vulnerable to perturbations in two specific patches. Masking out these two patches still leads to incorrect



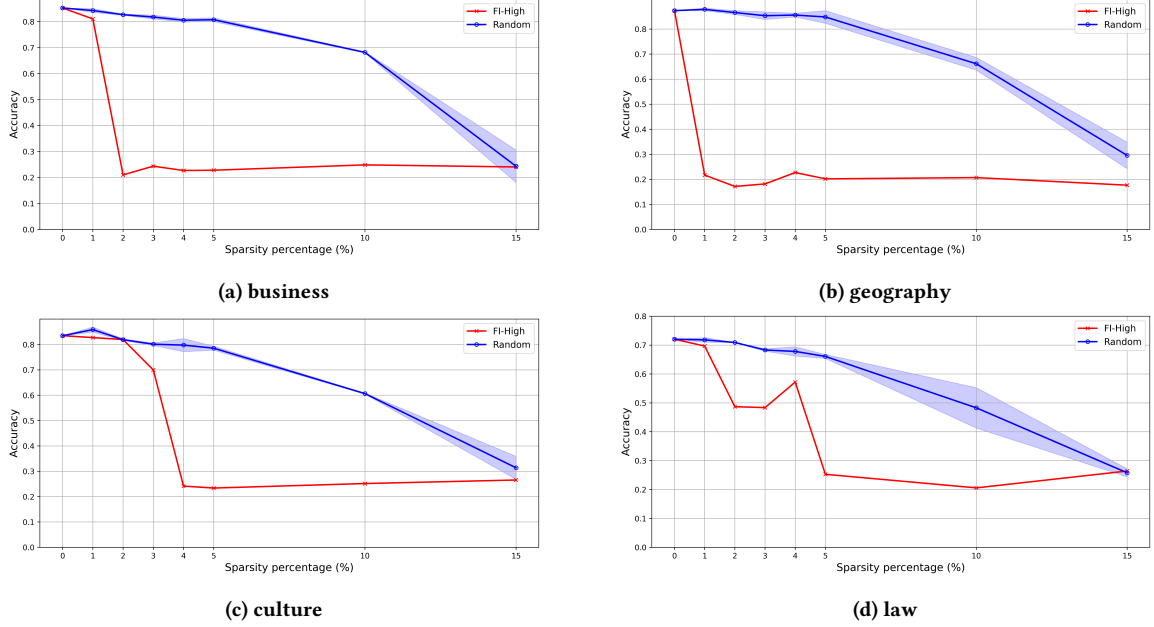


Figure 4: Comparing the accuracy in the MMLU dataset of Qwen2-7B when parameters have been sparsified at different rates.

Table 3: Performance of Different Models Based on Criteria with Full Value and Sparsity Percentages

Model	Criteria	Full	6% Sparsity		8% Sparsity		10% Sparsity		12% Sparsity	
			FI-High	Random	FI-High	Random	FI-High	Random	FI-High	Random
Llama2-13B	Rouge-1	1.0	0.52	0.59 ± 0.02	0.4	0.43 ± 0.06	0.18	0.68 ± 0.01	<u>0.05</u>	0.19 ± 0.03
	LCWR	0.43	0.38	0.41 ± 0.03	0.29	0.34 ± 0.07	<u>0.09</u>	0.42 ± 0.0	<u>0.01</u>	0.08 ± 0.05
Llama3-8B	Rouge-1	1.0	0.46	0.52 ± 0.04	0.21	0.41 ± 0.06	<u>0.09</u>	0.25 ± 0.04	<u>0.04</u>	0.12 ± 0.03
	LCWR	0.42	0.4	0.38 ± 0.01	0.12	0.30 ± 0.03	<u>0.0</u>	0.12 ± 0.01	<u>0.0</u>	0.01 ± 0.01
Llama2-7B	Rouge-1	1.0	0.44	0.56 ± 0.01	0.25	0.45 ± 0.02	<u>0.06</u>	0.33 ± 0.02	<u>0.0</u>	0.21 ± 0.02
	LCWR	0.42	0.32	0.4 ± 0.0	0.12	0.35 ± 0.01	<u>0.0</u>	0.19 ± 0.05	<u>0.0</u>	0.1 ± 0.03
Qwen2-7B	Rouge-1	1.0	<u>0.09</u>	0.41 ± 0.05	<u>0.01</u>	0.30 ± 0.09	<u>0.01</u>	0.31 ± 0.06	<u>0.01</u>	0.15 ± 0.02
	LCWR	0.41	<u>0.03</u>	0.35 ± 0.03	<u>0.02</u>	0.25 ± 0.1	<u>0.03</u>	0.20 ± 0.05	<u>0.03</u>	0.08 ± 0.02
Qwen2-1.5B	Rouge-1	1.0	0.18	0.4 ± 0.13	0.16	0.32 ± 0.02	<u>0.05</u>	0.28 ± 0.08	<u>0.05</u>	0.23 ± 0.02
	LCWR	0.14	<u>0.03</u>	0.07 ± 0.04	<u>0.04</u>	0.02 ± 0.02	<u>0.0</u>	0.04 ± 0.0	<u>0.0</u>	0.02 ± 0.02

merges these vectors linearly before adding back the base model:

$$\theta_{\text{Task}} = \theta_{\text{Base}} + \gamma(\delta_A + \delta_B), \quad (7)$$

where  $\delta_A = \theta_A - \theta_{\text{Base}}$  and similarly for  $\delta_B$ .

Both Average Merging and Task Arithmetic modify all parameters in models  $A$  and  $B$ , potentially degrading performance by disturbing their most sensitive parameters. To address this, we employ a protection strategy that preserves these vulnerable parameters while merging only the less critical ones. Specifically, we identify the top  $k\%$  of high-FI parameters in both models and record their locations in  $\Theta_A$  and  $\Theta_B$ . Then, for each layer in both  $\theta_{\text{Task}}$  and  $\theta_{\text{Avg}}$ , we revert parameters at locations in  $\Theta_A \cap \Theta_B^c$  to their

original values from  $\theta_A$ , and parameters at locations in  $\Theta_B \cap \Theta_A^c$  to their original values from  $\theta_B$ .

**TIES (TrIm, Elect Sign)** operates in two steps. First, it reduces redundancy by setting a fraction of the “task vectors”  $\delta_A$  and  $\delta_B$  to zero. Then, for each remaining entry, it retains the weight from the vector with the larger absolute value.

FI-guided protection can be incorporated into both steps. In the first step, we protect  $\delta_A$  at locations  $\Theta_A$  and  $\delta_B$  at  $\Theta_B$  from being trimmed. In the second step, entries within  $\Theta_A$  are preserved as  $\delta_A$ , while those in  $\Theta_B$  remain as  $\delta_B$ , regardless of their absolute values.

We merged **Qwen2.5-Math-7B** [48] and **HuatuoGPT-o1-7B** [8], as both models are further fine-tuned from the same base model,

**Qwen2.5-7B** [49]. The former is specifically fine-tuned for mathematical tasks, while the latter is tailored for medical and public health-related tasks. We evaluate the performance of the merged models on the math and health subjects within the MMLU benchmark [18].

From Table 4, we observe the following: (1) Across all merging methods, FI-guided protection generally enhances the performance of the merged models in both domains. This improvement occurs because protecting vulnerable parameters in both models helps mitigate performance degradation caused by parameter perturbation during merging. For example, the Average model merging method with FI-guided protection yields approximately a 1% improvement in both the Math and Health domains. (2) Furthermore, TIES with FI protection applied in its first stage performs the best among all merging methods, whereas DARE does not perform well in this setting.

Figure 5 uses average merging as an example. The results indicate that as the percentage of protected parameters increases, the performance of the merged models initially improves but later declines, highlighting a trade-off in FI-guided protection. Protecting a small proportion of parameters with the highest FI helps mitigate performance degradation caused by parameter conflicts. However, a high percentage of protection may lead to forgetting issues in both domains, as each protected location retains parameters from only one model, potentially limiting the integration of complementary knowledge. Thus, the protection percentage  $k$  serves as a crucial hyperparameter. To determine the optimal protection percentage, we conduct a hyperparameter search on the validation set. More details on hyperparameter selection can be found in Appendix A.2.

	FI-protection	Math	Health	Mean
Qwen2.5-Math-7B	/	0.616	/	/
HuatuogPT-o1-7B	/	/	0.724	/
Average	Without	0.534	0.514	0.524
	With	0.543	0.522	0.533
Task	Without	<u>0.577</u>	0.597	<u>0.587</u>
	With	0.573	<u>0.598</u>	0.586
TIES	Without	0.565	0.596	0.581
	With I	<b>0.583</b>	<b>0.606</b>	<b>0.595</b>
	With II	0.566	0.601	0.584
DARE-Task	/	0.573	0.589	0.581
DARE-TIES	/	0.560	0.588	0.574

**Table 4: Performance of merging Qwen2.5-Math-7B and HuatuogPT-o1-7B across both domains. The “Mean” column represents the average accuracy across the Math and Health domains, providing an overall performance measure. The best and second-best results in each domain are highlighted in bold and underlined fonts, respectively.**

## 6 Conclusion, Limitations & Discussion

This paper unveils the presence of cracks in the armor of LLMs, which poses challenges for quantifying the stability of LLMs under perturbations. To address this issue, we introduce a novel framework for adversarial learning that evaluates the stability of each

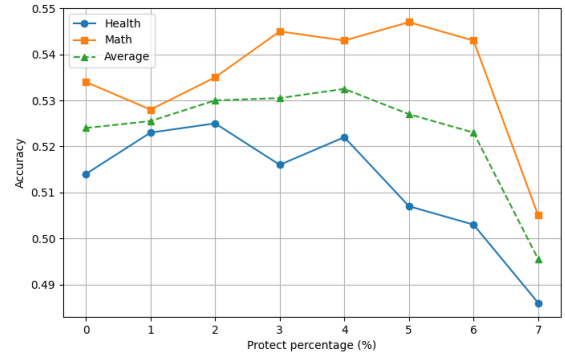


**Figure 5: Accuracy of average-merged models with FI-guided protection across both domains for different protection percentages  $k$ .**

component within LLMs, considering the impact of small perturbations on the overall system. Through experiments under both internal and external perturbations, we demonstrate the effectiveness of our proposed method.

Our method relies on gradient information and is not applicable to “black-box” models that do not expose internal parameters or gradients to users. In such cases, text-only approaches like Influence Function [23] are more suitable. While our method is computationally less expensive than second-order approaches such as Fisher Information [24] and Sharpness [13], an important direction for future work is to develop techniques that further accelerate the computation of the metric.

This paper focuses on evaluating the stability of LLMs under both external and internal perturbations at the inference stage. Extending our approach to the training stage presents a valuable research avenue. By adapting and expanding our FI metric, we can gain deeper insights into parameter stability during training, ultimately facilitating more efficient parameter fine-tuning and pre-training.

## References

- [1] Josh Achiam, Steven Adler, Sandhini Agarwal, Lama Ahmad, Ilge Akkaya, Florencia Leoni Aleman, Diogo Almeida, Janko Altenschmidt, Sam Altman, Shyamal Anadkat, et al. 2023. Gpt-4 technical report. *arXiv preprint arXiv:2303.08774* (2023).
- [2] Saleh Ashkboos, Maximilian L Croci, Marcelo Gennari do Nascimento, Torsten Hoeffler, and James Hensman. 2024. Slicept: Compress large language models by deleting rows and columns. *arXiv preprint arXiv:2401.15024* (2024).
- [3] Jinze Bai, Shuai Bai, Shusheng Yang, Shijie Wang, Sinan Tan, Peng Wang, Junyang Lin, Chang Zhou, and Jingren Zhou. 2023. Qwen-vl: A frontier large vision-language model with versatile abilities. *arXiv preprint arXiv:2308.12966* (2023).
- [4] Luke Bailey, Euan Ong, Stuart Russell, and Scott Emmons. 2023. Image hijacks: Adversarial images can control generative models at runtime. *arXiv preprint arXiv:2309.00236* (2023).
- [5] Stella Biderman, Hailey Schoelkopf, Quentin Gregory Anthony, Herbie Bradley, Kyle O’Brien, Eric Hallahan, Mohammad Aflah Khan, Shivanshu Purohit, USVSN Sai Prashanth, Edward Raff, et al. 2023. Pythia: A suite for analyzing large language models across training and scaling. In *International Conference on Machine Learning*. PMLR, 2397–2430.
- [6] Tom Brown, Benjamin Mann, Nick Ryder, Melanie Subbiah, Jared D Kaplan, Prafulla Dhariwal, Arvind Neelakantan, Pranav Shyam, Girish Sastry, Amanda Askell, et al. 2020. Language models are few-shot learners. *Advances in neural information processing systems* 33 (2020), 1877–1901.



- [7] Nicholas Carlini, Milad Nasr, Christopher A Choquette-Choo, Matthew Jagielski, Irena Gao, Pang Wei Koh, Daphne Ippolito, Florian Tramèr, and Ludwig Schmidt. 2024. Are aligned neural networks adversarially aligned? *Advances in Neural Information Processing Systems* 36 (2024).
- [8] Junying Chen, Zhenyang Cai, Ke Ji, Xidong Wang, Wanlong Liu, Rongsheng Wang, Jianye Hou, and Benyou Wang. 2024. Huatuogpt-o1, towards medical complex reasoning with llms. *arXiv preprint arXiv:2412.18925* (2024).
- [9] R Dennis Cook. 1986. Assessment of local influence. *Journal of the Royal Statistical Society Series B: Statistical Methodology* 48, 2 (1986), 133–155.
- [10] Laurent Dinh, Razvan Pascanu, Samy Bengio, and Yoshua Bengio. 2017. Sharp minima can generalize for deep nets. In *International Conference on Machine Learning*. PMLR, 1019–1028.
- [11] Abhimanyu Dubey, Abhinav Jauhri, Abhinav Pandey, Abhishek Kadian, Ahmad Al-Dahle, Aiesha Letman, Akhil Mathur, Alan Schelten, Amy Yang, Angela Fan, et al. 2024. The llama 3 herd of models. *arXiv preprint arXiv:2407.21783* (2024).
- [12] Yann Dubois, Balázs Galambosi, Percy Liang, and Tatsunori B Hashimoto. 2024. Length-controlled alpacaEval: A simple way to debias automatic evaluators. *arXiv preprint arXiv:2404.04475* (2024).
- [13] Pierre Foret, Ariel Kleiner, Hossein Mobahi, and Behnam Neyshabur. 2020. Sharpness-aware minimization for efficiently improving generalization. *arXiv preprint arXiv:2010.01412* (2020).
- [14] Stanislav Fort. 2023. Scaling laws for adversarial attacks on language model activations. *arXiv preprint arXiv:2312.02780* (2023).
- [15] Elias Frantar and Dan Alistarh. 2023. SparseGPT: Massive language models can be accurately pruned in one-shot. In *International Conference on Machine Learning*. PMLR, 10323–10337.
- [16] Samuel Gehman, Suchin Gururangan, Maarten Sap, Yejin Choi, and Noah A Smith. 2020. Realltoxicityprompts: Evaluating neural toxic degeneration in language models. *arXiv preprint arXiv:2009.11462* (2020).
- [17] Jonas Geiping, Alex Stein, Manli Shu, Khalid Saifullah, Yuxin Wen, and Tom Goldstein. 2024. Coercing LLMs to do and reveal (almost) anything. *arXiv preprint arXiv:2402.14020* (2024).
- [18] Dan Hendrycks, Collin Burns, Steven Basart, Andy Zou, Mantas Mazeika, Dawn Song, and Jacob Steinhardt. 2020. Measuring massive multitask language understanding. *arXiv preprint arXiv:2009.03300* (2020).
- [19] Yangsibo Huang, Samyak Gupta, Mengzhou Xia, Kai Li, and Danqi Chen. 2023. Catastrophic jailbreak of open-source llms via exploiting generation. *arXiv preprint arXiv:2310.06987* (2023).
- [20] Gabriel Ilharco, Marco Tulio Ribeiro, Mitchell Wortsman, Suchin Gururangan, Ludwig Schmidt, Hannaneh Hajishirzi, and Ali Farhadi. 2022. Editing models with task arithmetic. *arXiv preprint arXiv:2212.04089* (2022).
- [21] Albert Q Jiang, Alexandre Sablayrolles, Arthur Mensch, Chris Bamford, Devendra Singh Chaplot, Diego de las Casas, Florian Bressand, Gianna Lengyel, Guillaume Lample, Lucile Saulnier, et al. 2023. Mistral 7B. *arXiv preprint arXiv:2310.06825* (2023).
- [22] Ayush Kaushal, Tejas Vaidhya, and Irina Rish. 2023. Lord: Low rank decomposition of monolingual code llms for one-shot compression. *arXiv preprint arXiv:2309.14021* (2023).
- [23] Pang Wei Koh and Percy Liang. 2017. Understanding black-box predictions via influence functions. In *International conference on machine learning*. PMLR, 1885–1894.
- [24] Denis Kuznedelev, Eldar Kurtić, Elias Frantar, and Dan Alistarh. 2024. Cap: Correlation-aware pruning for highly-accurate sparse vision models. *Advances in Neural Information Processing Systems* 36 (2024).
- [25] Junyi Li, Jie Chen, Ruiyang Ren, Xiaoxue Cheng, Wayne Xin Zhao, Jian-Yun Nie, and Ji-Rong Wen. 2024. The dawn after the dark: An empirical study on factuality hallucination in large language models. *arXiv preprint arXiv:2401.03205* (2024).
- [26] Zeyi Liao and Huan Sun. 2024. AmplegCG: Learning a universal and transferable generative model of adversarial suffixes for jailbreaking both open and closed llms. *arXiv preprint arXiv:2404.07921* (2024).
- [27] Chris Yuhao Liu, Yaxuan Wang, Jeffrey Flanigan, and Yang Liu. 2024. Large Language Model Unlearning via Embedding-Corrupted Prompts. *arXiv preprint arXiv:2406.07933* (2024).
- [28] Haotian Liu, Chunyuan Li, Qingyang Wu, and Yong Jae Lee. 2024. Visual instruction tuning. *Advances in neural information processing systems* 36 (2024).
- [29] Qiang Liu, Lihong Li, Ziyang Tang, and Dengyong Zhou. 2018. Breaking the curse of horizon: Infinite-horizon off-policy estimation. *Advances in neural information processing systems* 31 (2018).
- [30] Xiaogeng Liu, Nan Xu, Muhao Chen, and Chaowei Xiao. 2023. Autodan: Generating stealthy jailbreak prompts on aligned large language models. *arXiv preprint arXiv:2310.04451* (2023).
- [31] Yuan Liu, Haodong Duan, Yuanhan Zhang, Bo Li, Songyang Zhang, Wangbo Zhao, Yike Yuan, Jiaqi Wang, Conghui He, Ziwei Liu, et al. 2024. Mmbench: Is your multi-modal model an all-around player?. In *European conference on computer vision*. Springer, 216–231.
- [32] Pan Lu, Swaroop Mishra, Tanglin Xia, Liang Qiu, Kai-Wei Chang, Song-Chun Zhu, Oyvind Tafjord, Peter Clark, and Ashwin Kalyan. 2022. Learn to explain: Multi-modal reasoning via thought chains for science question answering. *Advances in Neural Information Processing Systems* 35 (2022), 2507–2521.
- [33] Xinyin Ma, Gongfan Fang, and Xinchao Wang. 2023. Llm-pruner: On the structural pruning of large language models. *Advances in neural information processing systems* 36 (2023), 21702–21720.
- [34] Xin Men, Mingyu Xu, Qingyu Zhang, Bingning Wang, Hongyu Lin, Yaojie Lu, Xianpei Han, and Weipeng Chen. 2024. Shortgpt: Layers in large language models are more redundant than you expect. *arXiv preprint arXiv:2403.03853* (2024).
- [35] Roman Novak, Yasaman Bahri, Daniel A Abolafia, Jeffrey Pennington, and Jascha Sohl-Dickstein. 2018. Sensitivity and generalization in neural networks: an empirical study. *arXiv preprint arXiv:1802.08760* (2018).
- [36] Ethan Perez, Saffron Huang, Francis Song, Trevor Cai, Roman Ring, John Aslanides, Amelia Glaese, Nat McAleese, and Geoffrey Irving. 2022. Red teaming language models with language models. *arXiv preprint arXiv:2202.03286* (2022).
- [37] Xiangyu Qi, Kaixuan Huang, Ashwinee Panda, Peter Henderson, Mengdi Wang, and Prateek Mittal. 2024. Visual adversarial examples jailbreak aligned large language models. In *Proceedings of the AAAI Conference on Artificial Intelligence*, Vol. 38. 21527–21536.
- [38] Xiangyu Qi, Kaixuan Huang, Ashwinee Panda, Mengdi Wang, and Prateek Mittal. 2023. Visual adversarial examples jailbreak large language models. *arXiv preprint arXiv:2306.13213* (2023).
- [39] Christian Schlarmann and Matthias Hein. 2023. On the adversarial robustness of multi-modal foundation models. In *Proceedings of the IEEE/CVF International Conference on Computer Vision*. 3677–3685.
- [40] Hai Shu and Hongtu Zhu. 2019. Sensitivity analysis of deep neural networks. In *Proceedings of the AAAI Conference on Artificial Intelligence*, Vol. 33. 4943–4950.
- [41] Karen Simonyan, Andrea Vedaldi, and Andrew Zisserman. 2013. Deep inside convolutional networks: Visualising image classification models and saliency maps. *arXiv preprint arXiv:1312.6034* (2013).
- [42] C Szegegy. 2013. Intriguing properties of neural networks. *arXiv preprint arXiv:1312.6199* (2013).
- [43] Hugo Touvron, Thibaut Lavril, Gautier Izacard, Xavier Martinet, Marie-Anne Lachaux, Timothée Lacroix, Baptiste Rozière, Naman Goyal, Eric Hambro, Faisal Azhar, et al. 2023. Llama: Open and efficient foundation language models. *arXiv preprint arXiv:2302.13971* (2023).
- [44] Rey Wiyatno and Anqi Xu. 2018. Maximal jacobian-based saliency map attack. *arXiv preprint arXiv:1808.07945* (2018).
- [45] Mitchell Wortsman, Gabriel Ilharco, Samir Ya Gadre, Rebecca Roelofs, Raphael Gontijo-Lopes, Ari S Morcos, Hongseok Namkoong, Ali Farhadi, Yair Carmon, Simon Kornblith, et al. 2022. Model soups: Averaging weights of multiple fine-tuned models improves accuracy without increasing inference time. In *International conference on machine learning*. PMLR, 23965–23998.
- [46] Zhongbin Xie and Thomas Lukasiewicz. 2023. An empirical analysis of parameter-efficient methods for debiasing pre-trained language models. *arXiv preprint arXiv:2306.04067* (2023).
- [47] Prateek Yadav, Derek Tam, Leshem Choshen, Colin A Raffel, and Mohit Bansal. 2024. Ties-merging: Resolving interference when merging models. *Advances in Neural Information Processing Systems* 36 (2024).
- [48] An Yang, Baosong Yang, Beichen Zhang, Binyuan Hui, Bo Zheng, Bowen Yu, Chengyuan Li, Dayiheng Liu, Fei Huang, Haoran Wei, et al. 2024. Qwen2. 5 technical report. *arXiv preprint arXiv:2412.15115* (2024).
- [49] An Yang, Beichen Zhang, Binyuan Hui, Bofei Gao, Bowen Yu, Chengpeng Li, Dayiheng Liu, Jianhong Tu, Jingren Zhou, Junyang Lin, et al. 2024. Qwen2. 5-math technical report: Toward mathematical expert model via self-improvement. *arXiv preprint arXiv:2409.12122* (2024).
- [50] Enneng Yang, Li Shen, Guibing Guo, Xingwei Wang, Xiaochun Cao, Jie Zhang, and Dacheng Tao. 2024. Model merging in llms, mllms, and beyond: Methods, theories, applications and opportunities. *arXiv preprint arXiv:2408.07666* (2024).
- [51] Le Yu, Bowen Yu, Haiyang Yu, Fei Huang, and Yongbin Li. 2024. Language models are super mario: Absorbing abilities from homologous models as a free lunch. In *Forty-first International Conference on Machine Learning*.
- [52] Youliang Yuan, Wenxiang Jiao, Wenxuan Wang, Jen-tse Huang, Pinjia He, Shuming Shi, and Zhaopeng Tu. 2023. Gpt-4 is too smart to be safe: Stealthy chat with llms via cipher. *arXiv preprint arXiv:2308.06463* (2023).
- [53] Xinyu Zhang, Huiyu Xu, Zhongjie Ba, Zhibo Wang, Yuan Hong, Jian Liu, Zhan Qin, and Kui Ren. 2024. Privacyasst: Safeguarding user privacy in tool-using large language model agents. *IEEE Transactions on Dependable and Secure Computing* (2024).
- [54] Yunqing Zhao, Tianyu Pang, Chao Du, Xiao Yang, Chongxuan Li, Ngai-Man Man Cheung, and Min Lin. 2024. On evaluating adversarial robustness of large vision-language models. *Advances in Neural Information Processing Systems* 36 (2024).
- [55] Hongtu Zhu, Joseph G Ibrahim, Sikyung Lee, and Heping Zhang. 2007. Perturbation selection and influence measures in local influence analysis. 35 (2007), 2565–2588.
- [56] Hongtu Zhu, Joseph G Ibrahim, and Niansheng Tang. 2011. Bayesian influence analysis: a geometric approach. *Biometrika* 98, 2 (2011), 307–323.
- [57] Andy Zou, Zifan Wang, J Zico Kolter, and Matt Fredrikson. 2023. Universal and Transferable Adversarial Attacks on Aligned Language Models. *arXiv preprint arXiv:2307.15043* (2023).

## A Appendices

### A.1 Detail of Parameter sparsification experiment

**Experiment on MMLU** We conduct experiments on the multiple-choice problems from the MMLU [18] dataset, using Qwen2-7B. We take the cross-entropy loss, *i.e.*,  $f = -\log P(y = y_{\text{pred}}|x, \theta)$ , as the target function, and calculate the FI value according to Theorem 3.4. In this setup, we treat the task as a 4-class classification problem with the possible classes being "A," "B," "C," and "D".

**Experiment on Alpaca-Eval** We use the Alpaca-eval validation set [12], a widely adopted benchmark, and conduct experiments with various open-source models, including LLaMA2, LLaMA3 [43], and Qwen2 [3], across different sizes. We report two metrics: ROUGE-1 (comparing to pre-sparsity responses) and length-control winning rate (LCWR), comparing to GPT-3.5 Turbo. Higher scores are better for both metrics.

To estimate the average Fisher Information (FI) for sequence generation, we use the fixed-context approach with  $L = 5$ . For each sample  $z$ , we estimate  $\text{FI}_l(z)$  by generating  $N = 10$  responses, truncating them at position  $l - 1$ . These truncated sequences are used to approximate the conditional expectation in Equation 5 by computing the sample average. The per-token FI values are then aggregated using Equation 6 to obtain  $\text{FI}_{\text{seq}}^L(z)$ , which is averaged across all samples to estimate the overall FI.

### A.2 Detail of FI-guided protection in model merging

See Table 5.

**Table 5: Searched ranges of hyperparameters of model merging methods**

Hyper parameter	Search Ranges of Hyperparameters
Protecting ratio $k$	[1%, 2%, 3%, 4%, 5%, 6%, 7%, 8%, 9%, 10%]
Weight parameter $\gamma$ in Equation 7 & TIES	[0.3, 0.4, 0.5, 0.6, 0.9, 1.0]

### A.3 Proof of Theorem 3.4

PROOF. We apply Taylor expansion to  $f(\omega(t))$  at the point  $\omega(t)$ :

$$f(\omega(t)) = f(\omega(0)) + \nabla_{f(\omega_0)}^T h_{\omega_0} t + \frac{1}{2} \left( h_{\omega_0}^T H_{f(\omega_0)} h_{\omega_0} + \nabla_{f(\omega_0)}^T d^2 \omega(0)/dt^2 \right) t^2 + o(t^2),$$

where  $\nabla_{f(\omega_0)} = \partial f(\omega) / \partial \omega|_{\omega=\omega_0}$  and  $H_{f(\omega_0)} = \partial^2 f(\omega) / \partial \omega \partial \omega^T|_{\omega=\omega_0}$ . From Equation 3,  $S_C^2(\omega_t, \omega_0)$  can be approximated as  $S_C^2(\omega_t, \omega_0) = t^2 h_{\omega_0}^T G_{\omega_0} h_{\omega_0} + o(t^2)$ . Based on l'Hopital's rule, the stability measure FI from Equation 2 can be rewritten as:

$$\text{FI}_{\omega}(\omega_0) = \max_{h_{\omega}} \frac{h_{\omega}^T \nabla_{f(\omega_0)} \nabla_{f(\omega_0)}^T h_{\omega}}{h_{\omega}^T G_{\omega_0} h_{\omega}}.$$

We then reparameterize  $\omega$  to  $\tilde{\omega} = G_{\omega_0}^{-1/2} \omega$ . According to Theorem 3.3, the stability measure FI remains invariant under this reparameterization

$$\text{FI}_{\omega}(\omega_0) = \text{FI}_{\tilde{\omega}}(\tilde{\omega}_0) = \arg \max_{h_{\tilde{\omega}}} \frac{h_{\tilde{\omega}}^T G_{\omega_0}^{-1/2} \nabla_{f(\omega_0)} \nabla_{f(\omega_0)}^T G_{\omega_0}^{-1/2} h_{\tilde{\omega}}}{h_{\tilde{\omega}}^T h_{\tilde{\omega}}}.$$

The maximization problem is now in the form of a Rayleigh quotient, which attains its maximum when  $h_{\tilde{\omega}}$  is proportional to  $G_{\omega_0}^{-1/2} \nabla_{f(\omega_0)}$ . Substituting back into the Rayleigh quotient, we find:

$$\begin{aligned} \text{FI}_{\omega}(\omega_0) &= \frac{\left( G_{\omega_0}^{-1/2} \nabla_{f(\omega_0)} \right)^T G_{\omega_0}^{-1/2} \nabla_{f(\omega_0)} \nabla_{f(\omega_0)}^T G_{\omega_0}^{-1/2} \left( G_{\omega_0}^{-1/2} \nabla_{f(\omega_0)} \right)}{\left( G_{\omega_0}^{-1/2} \nabla_{f(\omega_0)} \right)^T \left( G_{\omega_0}^{-1/2} \nabla_{f(\omega_0)} \right)} \\ &= \frac{\nabla_{f(\omega_0)}^T G_{\omega_0}^{-1} \nabla_{f(\omega_0)} \nabla_{f(\omega_0)}^T G_{\omega_0}^{-1} \nabla_{f(\omega_0)}}{\nabla_{f(\omega_0)}^T G_{\omega_0}^{-1} \nabla_{f(\omega_0)}} \\ &= \nabla_{f(\omega_0)}^T G_{\omega_0}^{-1} \nabla_{f(\omega_0)}. \end{aligned}$$

This concludes the proof.  $\square$